Extrapolation of MIMO Mobile-to-Mobile Wireless Channels Using Parametric-Model-Based Prediction

Ramoni O. Adeogun, *Member, IEEE*, Paul D. Teal, *Senior Member, IEEE*, and Pawel A. Dmochowski, *Senior Member, IEEE*

***Abstract*—This paper investigates the prediction of multiple-input–multiple-output (MIMO) narrow-band multipath fading channels for mobile-to-mobile (M-to-M) wireless communication systems. Using a statistical model for M-to-M communication in urban and suburban environments, we derive a parameterized double directional model and utilize a multidimensional extension of the ESPRIT algorithm to jointly estimate the angles of departure (AoD), angles of arrival (AoA), and effective Doppler frequencies. A simple method is also proposed for mobile velocity estimation. The parameter estimates are then used to forecast the M-to-M channel. The bound on the prediction error is derived using a vector formulation of the Cramer–Rao lower bound (CRLB). Simulations are used to evaluate the performance of the prediction scheme and to compare it to the derived error bound.**

***Index Terms*—Channel estimation and prediction Cramer–Rao bound, estimation of signal parameters via rotational invariance techniques (ESPRIT), mobile-to-mobile (M-to-M) channel, multidimensional parameter estimation, multiple-input–multiple-output (MIMO), multipath fading channels.**

I. Introduction

MOBILE-to-mobile (M-to-M) land wireless communication channels arise when both the transmitter and receiver are moving and are equipped with low-elevation antenna elements. For instance, a moving vehicle in a given location might communicate with one or more mobile vehicles in other locations. These systems have potential applications in traffic safety, rescue squad communication, congestion avoidance, etc. An international wireless standard, i.e., IEEE 802.11p, which is also referred to as Wireless Access in Vehicular Environments (WAVE), has been developed [1]. Based on Wi-Fi technology, this standard is proposed for both mobile-to-mobile and mobile-to-infrastructure traffic applications.

To cope with the challenge of developing and evaluating the performance of current and future M-to-M wireless communication systems, several research results have been published on the modeling of single-input–single-output (SISO) M-to-M channels. In [2] and [3], the statistical properties of such channels were investigated based on models for the channel impulse response and the transfer function. In [4], results on the temporal correlation properties and Doppler power spectral characteristics in 3-D propagation environments were presented. In [5] and [6], a modeling technique based on ray-tracing was used to model the vehicle-to-vehicle propagation channels. The proposed channel impulse responses capture the channel statistics in terms of time series and can therefore be used directly for link- and system-level simulations. Results based on measurement for outdoor-to-outdoor, outdoor-to-indoor, and wideband M-to-M wireless channels have also been presented in [7]–[9]. Simulation models for SISO M-to-M channel were presented in [10]. These results have shown that the fading statistics of M-to-M channels differ significantly from classical fixed-to-mobile (F-to-M) channels.

Recently, modeling of M-to-M channels with multiple-antenna elements at both ends of the link has received considerable research attention. In [11] and [12], the statistical model for SISO M-to-M channel was extended to multiple-input–multiple-output (MIMO) M-to-M channels. The scattering environment was modeled around the mobile transmitter and receiver using the classical two-ring geometrical channel model. Simulation models were developed for MIMO M-to-M channels in [13]. In [14] and [15], the 2-D M-to-M models in [13] were extended to the modeling of 3-D (azimuth and elevation) propagation scenarios. In [16], techniques for the computation of channel parameters for MIMO transmission channels with dual mobility were proposed. The schemes developed were based on a Rayleigh fading channel envelope with nonisotropic scattering. Comprehensive reviews of existing channel models, measurement campaign, and other aspects of MIMO M-to-M channel modeling can be found in [17].

Although multipath parameter estimation and channel state prediction has been thoroughly addressed for F-to-M MIMO channels (see, e.g., [18]–[23]), there exist very few publications (to the best of the authors' knowledge) applicable to M-to-M MIMO systems. In [24], a maximum likelihood approach for MIMO M-to-M channel parameter estimation was developed. The computational burden and dependence on the channel model, however, makes the scheme expensive for practical applications. In [25] and [26], schemes for the estimation of mobile velocities and direction of motion were proposed for SISO M-to-M channels. The proposed scheme is, however, limited to the two-ring model, and extension to MIMO channels is still an open problem.

Manuscript received March 13, 2014; revised July 10, 2014 and October 12, 2014; accepted October 29, 2014. Date of publication November 4, 2014; date of current version October 13, 2015. The review of this paper was coordinated by Prof. Y. Gong.

The authors are with the School of Engineering and Computer Science, Victoria University of Wellington, Wellington 6140, New Zealand (e-mail: ramoni.adeogun@ecs.vuw.ac.nz; paul.teal@ecs.vuw.ac.nz; pawel.dmochowski@ecs.vuw.ac.nz).

Color versions of one or more of the figures in this paper are available online at http://ieeexplore.ieee.org.

Digital Object Identifier 10.1109/TVT.2014.2366757

In this paper, we investigate the prediction of MIMO M-to-M channel fading channels. It is well known from [27]–[29] that channel prediction offers significant benefits in mitigating performance loss from multipath fading and improving the system performance by providing both the transmitter and receiver with an accurate forecast of the channel impulse response. We believe that this fact, coupled with the faster variation exhibited by M-to-M channels, make channel prediction an important open problem. The contributions of this paper are as follows.

- Based on a statistical model of the narrow-band M-to-M channel, we derive a generalized parametric model for parameter extraction and extrapolation of MIMO M-to-M channels.
- Since the number of antenna elements in practical systems is less than the number of propagation paths, we propose a simple transformation that converts the observed channel response into a sufficiently large multidimensional observation matrix exhibiting translational invariance in all dimensions.
- An adaptation of the computationally efficient subspace-based estimation of signal parameters via rotational invariance techniques (ESPRIT) is presented to jointly extract the angles of arrival (AOAs), angles of departure (AODs), and effective Doppler frequencies from the transformed data matrix. The parameters are used for channel extrapolation.
- Using the estimated channel parameters, a least squares (LS) approach is proposed for the estimation of the transmitter and receiver velocity.
- Expressions for the lower bound on the estimation and prediction error are derived. This is achieved using a vector formulation of the Cramer–Rao lower bound (CRLB).

The remainder of this paper is organized as follows. In Section II, we present a statistical model for M-to-M channels and derive a simple model for parameter estimation and prediction. Details of data preprocessing and the parametric models necessary for joint estimation of the channel parameters are presented in Section III. In Section IV, we describe the ESPRIT-based approach for jointly estimating the channel parameters along with LS amplitude estimation and the parametric prediction. We present a derivation of the bound on prediction error in Section V, whereas Section VI presents results of numerical simulations. Finally, conclusions are drawn in Section VII.

II. Channel Models

Here, we present the Rayleigh fading narrow-band MIMO M-to-M channel model considered in this paper along with a parametrized model for M-to-M parameter estimation and prediction.

A. MIMO M-to-M Channel Model

We consider a MIMO M-to-M wireless system with M transmit and N receive antenna elements. Fig. 1 shows an illustration of M-to-M propagation in a typical urban and suburban environment. The transmitter and receiver are assumed moving with velocities v_t and v_r, respectively. It is further assumed that

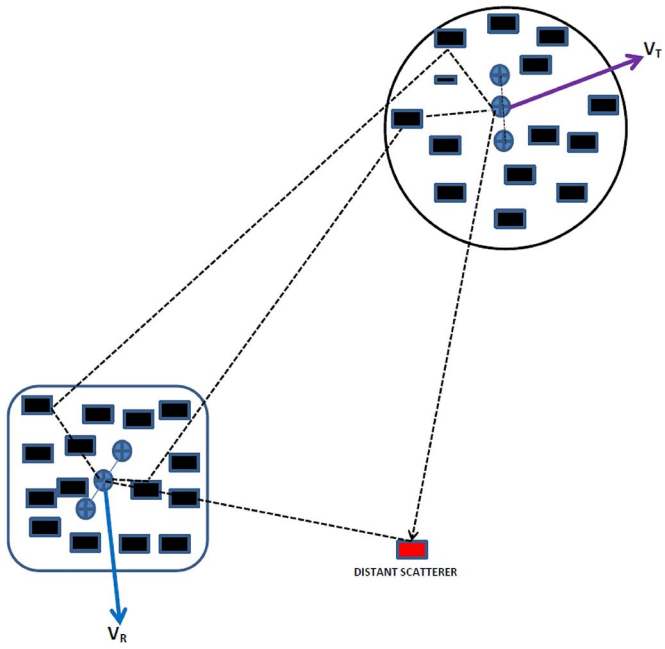

Fig. 1. A 3×3 MIMO M-to-M wireless propagation channel characterized by local scatterers around both the transmitter and receiver and distant scattering sources.

both are equipped with low-elevation omnidirectional antennas. As shown in Fig. 1, a signal will arrive at the receiver after undergoing scattering and reflection in all directions by local objects near the transmitter and receiver, as well as distant scattering objects. We assume a non-line-of-sight propagation environment; therefore, the complex Rayleigh faded channel for a SISO link is modeled as [2], [3]

$$h(t) = \sum_{k=1}^{K} \alpha_k e^{j\left[\left(\omega_k^t + \omega_k^r\right)t + \phi_k\right]} \tag{1}$$

where α_k is the amplitude for the kth path, ϕ_k is the kth path phase parameter assumed uniformly distributed on $[0, 2\pi[$, and K is the number of propagation paths. ω_k^t and ω_k^r are the radian Doppler shifts resulting from the mobility of the transmitter and receiver, respectively, and are given by

$$\omega_k^t = \frac{2\pi}{\lambda} v_t \sin\left(\vartheta_k^t\right) \tag{2}$$

$$\omega_k^r = \frac{2\pi}{\lambda} v_t \sin\left(\vartheta_k^r\right) \tag{3}$$

where ϑ_k^t is the angle between the direction of departure of the kth path and the transmitter direction of motion. ϑ_k^r is the corresponding angle at the receive array, and λ is the carrier wavelength. As shown in (1), the received signal will experience Doppler frequency shifts due to the mobility of both the transmitter and receiver. The dual mobility in M-to-M channels results in more rapid temporal variation of the fading envelope when compared with classical mobile cellular systems with fixed transmitters. It should be noted that the sum of sinusoids model commonly used for SISO prediction studies (see, e.g., [28], [30]–[32]) is a special case of (1) with $v_t = 0$. The model in (1) can be extended to M-to-M communication

channels with multiple antennas at both ends of the link by introducing the receive and transmit spatial structure, giving

$$\mathbf{H}(t) = \sum_{k=1}^{K} \alpha_k \mathbf{a}_r\left(\theta_k^r\right) \mathbf{a}_t^T\left(\theta_k^t\right) e^{j\left[\left(\omega_k^t+\omega_k^r\right)t+\phi_k\right]} \tag{4}$$

where $[\cdot]^T$ denotes the transpose operation, $\mathbf{a}_r(\theta_k^r)$ and $\mathbf{a}_t(\theta_k^t)$ are the array-geometry-dependent receive and transmit steering vectors, respectively, and θ_k^r and θ_k^t are the AoA and AoD of the kth path relative to the array broadside, respectively. For a uniform linear array (ULA), the receive array steering vector is defined as

$$\mathbf{a}_r\left(\theta_k^r\right) = \begin{bmatrix} 1 & e^{-j2\pi\delta r \sin\theta_k^r} & \cdots & e^{-j2\pi(N-1)\delta r \sin\theta_k^r} \end{bmatrix}^T \tag{5}$$

where δr is the receiving mobile antenna spacing. The transmit array steering is analogously obtained from (5) by replacing θ_k^r with θ_k^t, N with M and δr with δt.

B. Parametrized Model

We now reduce the MIMO M-to-M channel prediction problem to a multidimensional sinusoidal parameter estimation problem. In doing so, we define

$$\beta_k = \alpha_k \exp(j\phi_k) \tag{6}$$

$$\begin{aligned}\omega_k &= \omega_k^t + \omega_k^r \\ &= \frac{2\pi}{\lambda}\left(v_t \sin\left(\vartheta_k^t\right) + v_r \sin\left(\vartheta_k^r\right)\right).\end{aligned} \tag{7}$$

We will henceforth refer to β_k as the complex amplitude of the kth path and ω_k as the effective radian Doppler frequency. Substituting (6) and (7) into (4), we obtain

$$\mathbf{H}(t) = \sum_{k=1}^{K} \beta_k \mathbf{a}_r\left(\theta_k^r\right) \mathbf{a}_t^T\left(\theta_k^t\right) e^{j\omega_k t}. \tag{8}$$

The parameters β_k, θ_k^r, θ_k^t, and ω_k are assumed constant over the region of interest.[1] We also assume that L samples of the channel impulse response are known either by transmitting a known pilot sequence or from channel measurement. In practice, the estimated or measured channel will be imperfect due to the effects of noise and multiuser interference. We therefore model the known channel at time t as

$$\hat{\mathbf{H}}(t) = \mathbf{H}(t) + \mathbf{Z}(t) \tag{9}$$

where $\mathbf{H}(t)$ is the actual channel, and $\mathbf{Z}(t)$ is a random variable that accounts for the effects of noise and interference. For simplicity, we assume that $\mathrm{vec}(\mathbf{Z}(t)) \sim \mathcal{CN}(0, \sigma_z^2\mathbf{I})$.

[1]A rule of thumb for determining the validity range is given in [30] as

$$t_{\mathrm{valid}} = \sqrt{\frac{cr_{\min}}{3f_c v^2}}$$

where $r_{\min}$ is the distance between the mobile receiver and the nearest scattering source, $c = 3.0 \times 10^8$ m/s is the velocity of light, v is the mobile velocity, and f_c is the carrier frequency.

III. Data Preprocessing and Parameter Estimation Model

Prediction of the M-to-M MIMO channel using the model in (8) has been converted to a multiple sinusoidal parameter estimation problem. Here, we will present the data preprocessing required for the joint extraction of the parameters from the available noisy channel estimates and derive a model upon which the parameter estimation stage of the prediction algorithm will be based.

A. Data Preprocessing

We perform a vectorization operation on the noisy channel estimates by stacking the columns of the matrices to form

$$\begin{aligned}\hat{\mathbf{h}}(t) &= \mathrm{vec}\left[\mathbf{H}(t) + \mathbf{Z}(t)\right] \\ &= \sum_{k=1}^{K} \mathrm{vec}\left[\beta_k \mathbf{a}_r\left(\theta_k^r\right) \mathbf{a}_t^T\left(\theta_k^t\right) e^{j\omega_k t}\right] + \mathbf{z}(t)\end{aligned} \tag{10}$$

where $\mathbf{z}(t) = \mathrm{vec}[\mathbf{Z}(t)]$ is the vectorized version of the estimation noise matrix. Using the properties of the Kronecker product, it can be shown that the vectorized channel impulse response in (10) can be expressed as

$$\hat{\mathbf{h}}(t) = \sum_{k=1}^{K} \beta_k \mathbf{a}_r\left(\theta_k^r\right) \otimes \mathbf{a}_t\left(\theta_k^t\right) e^{j\omega_k t} + \mathbf{z}(t) \tag{11}$$

where $\otimes$ denotes the Kronecker product. Assuming that the channel is sampled with period Δt, the channel state information (CSI) at time instant ℓ is

$$\hat{\mathbf{h}}(\ell) = \sum_{k=1}^{K} \beta_k \mathbf{a}_r\left(\theta_k^r\right) \otimes \mathbf{a}_t\left(\theta_k^t\right) e^{j(\ell-1)\nu_k} + \mathbf{z}(\ell) \tag{12}$$

where $\nu_k = \omega_k \Delta t$ is the normalized radian Doppler frequency. Finally, we form a $NMS \times R$ Hankel data matrix

$$\mathbf{F} = \begin{bmatrix} \hat{\mathbf{h}}(1) & \hat{\mathbf{h}}(2) & \cdots & \hat{\mathbf{h}}(R) \\ \hat{\mathbf{h}}(2) & \hat{\mathbf{h}}(3) & \cdots & \hat{\mathbf{h}}(R+1) \\ \vdots & \vdots & \ddots & \vdots \\ \hat{\mathbf{h}}(S) & \hat{\mathbf{h}}(S+1) & \cdots & \hat{\mathbf{h}}(L) \end{bmatrix} \tag{13}$$

where R and S are the matrix size parameters, selected such that the smallest dimension of $\mathbf{F}$ is greater than the number of sources. This is necessary since the size of $\mathbf{F}$ determines the size of the covariance matrix to be defined in Section IV-A and, hence, the maximum number of resolvable sources.

B. Parameter Estimation Model

We will now derive a model for the transformed CSI as presented in $\mathbf{F}$ and show that it represents 3-D data corresponding

to the transmit and receive spatial dimensions and the temporal dimension of the channel. Let $\mathbf{a}_d(\nu_k)$ be a S-dimensional vector defined as

$$\mathbf{a}_d(\nu_k) = \begin{bmatrix} 1 & e^{j2\nu_k} & \cdots & e^{j(S-1)\nu_k} \end{bmatrix}^T. \tag{14}$$

Using the transformations in (13) and the model in (11), the ith column of $\mathbf{F}$ can be expressed as

$$\begin{aligned} \mathbf{f}(i) &= \sum_{k=1}^{K} \beta_k \left(\mathbf{a}_r\left(\theta_k^r\right) \otimes \mathbf{a}_t\left(\theta_k^t\right) \otimes \mathbf{a}_d(\nu_k) \right) e^{j(i-1)\nu_k} + \mathbf{z}(i) \\ &= \mathbf{A}(\boldsymbol{\theta}^r, \boldsymbol{\theta}^t, \boldsymbol{\nu})\boldsymbol{\beta}(i) + \mathbf{z}(i) \end{aligned} \tag{15}$$

where $\boldsymbol{\beta}(i) = [\beta_1 e^{j(i-1)\nu_1}, \beta_2 e^{(j(i-1)\nu_2}, \ldots, \beta_K e^{j(i-1)}\nu_K]^T$, and $\mathbf{A}(\boldsymbol{\theta}^r, \boldsymbol{\theta}^t, \boldsymbol{\nu}) = [\mathbf{a}_r(\theta_1^r) \otimes \mathbf{a}_t(\theta_1^t) \otimes \mathbf{a}_d(\nu_1), \ldots, \mathbf{a}_r(\theta_K^r) \otimes \mathbf{a}_t(\theta_K^t) \otimes \mathbf{a}_d(\nu_K)]$ is a $NMS \times R$ spatiotemporal manifold matrix. The model in (15) corresponds to a 3-D observation data and can be used to jointly estimate the AOA, AOD, and effective Doppler frequencies. We next present the procedure for the extraction of the parameters from the transformed data.

IV. Parameter Acquisition and Channel Prediction

The multipath parameter estimation step is divided into four stages: covariance matrix estimation; subspace dimension estimation; joint AOA, AOD, and Doppler frequency estimation; and amplitude estimation.

A. Covariance Matrix Estimation

The parameter estimation stage utilizes the eigenvalue decomposition (EVD) of the spatiotemporal covariance matrix, which is defined as

$$\begin{aligned} \hat{\mathbf{C}} &= \frac{\mathbf{F}\mathbf{F}^H}{R} \\ &= \frac{1}{R}\sum_{r=1}^{R} \mathbf{f}(i)\mathbf{f}(i)^H \\ &= \mathbf{A}(\boldsymbol{\theta}^r, \boldsymbol{\theta}^t, \boldsymbol{\nu})\mathbf{R}_{\beta\beta}\mathbf{A}^H(\boldsymbol{\theta}^r, \boldsymbol{\theta}^t, \boldsymbol{\nu}) + \sigma^2\mathbf{I} \end{aligned} \tag{16}$$

where $[\cdot]^H$ denotes the Hermitian transpose, and $\mathbf{R}_{\beta\beta} = (1/R)\sum_{r=1}^{R} \boldsymbol{\beta}\boldsymbol{\beta}^H$.

B. Subspace Dimension Estimation

Estimation of the number of dominant sources is an important step in any parameter estimation and prediction scheme. Common methods for estimating the number of signal sources are the minimum description length (MDL) [33] and the Akaike information criterion (AIC) [34]. We will apply a modified version of the MDL criterion referred to as minimum mean square error (MMSE)–MDL [35]. Let $\lambda_v, v = 1, 2, \ldots, NMS$ be the eigenvalues of $\hat{\mathbf{C}}$. The estimate of the signal subspace is given by [35]

$$\hat{K} = \underset{v=1,\ldots,V-1}{\operatorname{argmin}} \text{MMDL}(v) \tag{17}$$

where $V = NMS$, and $\text{MMDL}(v)$ is the MMSE–MDL criterion given by

$$\text{MMDL}(v) = R\log(\lambda_v) + \frac{1}{2}(v^2 + v)\log R. \tag{18}$$

C. Joint AOA, AOD, and Doppler Estimation

An adaptation of the rotational invariance technique ESPIRIT [36] and multiple invariance ESPRIT [37], [38] is presented here for the joint estimation of the AOA, AOD, and effective Doppler frequencies. Following the eigendecomposition of $\hat{\mathbf{C}}$, we separate the signal and noise subspaces. To exploit the rotational invariance structure in the spatiotemporal manifold matrix, we define the following 1-D and 3-D selection matrices for each of the three dimensions:

$$\begin{aligned} \mathbf{J}_{1r} &= \begin{bmatrix} \mathbf{I}_{(N-1)} & \mathbf{0}_{(N-1)} \end{bmatrix}, \quad \mathbf{J}_{r1} = \mathbf{I}_M \otimes \mathbf{I}_S \otimes \mathbf{J}_{1r} \\ \mathbf{J}_{2r} &= \begin{bmatrix} \mathbf{0}_{(N-1)} & \mathbf{I}_{(N-1)} \end{bmatrix}, \quad \mathbf{J}_{r2} = \mathbf{I}_M \otimes \mathbf{I}_S \otimes \mathbf{J}_{2r} \\ \mathbf{J}_{1t} &= \begin{bmatrix} \mathbf{I}_{(M-1)} & \mathbf{0}_{(M-1)} \end{bmatrix}, \quad \mathbf{J}_{t1} = \mathbf{I}_S \otimes \mathbf{J}_{1t} \otimes \mathbf{I}_N \\ \mathbf{J}_{2t} &= \begin{bmatrix} \mathbf{0}_{(M-1)} & \mathbf{I}_{(M-1)} \end{bmatrix}, \quad \mathbf{J}_{t2} = \mathbf{I}_S \otimes \mathbf{J}_{2t} \otimes \mathbf{I}_N \\ \mathbf{J}_{1d} &= \begin{bmatrix} \mathbf{I}_{(S-1)} & \mathbf{0}_{(S-1)} \end{bmatrix}, \quad \mathbf{J}_{d1} = \mathbf{J}_{1d} \otimes \mathbf{I}_N \otimes \mathbf{I}_M \\ \mathbf{J}_{2d} &= \begin{bmatrix} \mathbf{0}_{(S-1)} & \mathbf{I}_{(S-1)} \end{bmatrix}, \quad \mathbf{J}_{d2} = \mathbf{J}_{2d} \otimes \mathbf{I}_N \otimes \mathbf{I}_M \end{aligned} \tag{19}$$

where $\mathbf{I}_E$ is an $E \times E$ identity matrix, and $\mathbf{0}_E$ is a length E vector of zeros. Using the selection matrices in (19), we form the following invariance equations:

$$\begin{aligned} \mathbf{J}_{r2}\mathbf{U}_\text{s} &= \mathbf{J}_{r1}\mathbf{U}_\text{s}\boldsymbol{\Theta}^r \\ \mathbf{J}_{t2}\mathbf{U}_\text{s} &= \mathbf{J}_{t1}\mathbf{U}_\text{s}\boldsymbol{\Theta}^t \\ \mathbf{J}_{d2}\mathbf{U}_\text{s} &= \mathbf{J}_{d1}\mathbf{U}_\text{s}\boldsymbol{\Theta}^d \end{aligned} \tag{20}$$

where $\mathbf{U}_\text{s}$ is the $NMS \times \hat{K}$ signal subspace matrix with eigenvectors corresponding to the $\hat{K}$ largest eigenvalues of $\hat{\mathbf{C}}$ as its columns. The eigenvalues of $\boldsymbol{\Theta}^r$, $\boldsymbol{\Theta}^t$, and $\boldsymbol{\Theta}^d$ contain information about their respective parameters, i.e.,

$$\begin{aligned} \text{eig}(\boldsymbol{\Theta}^r) &= \text{diag}\begin{bmatrix} e^{j\mu_1^r} & \cdots & e^{j\mu_{\hat{K}}^r} \end{bmatrix} \\ \text{eig}(\boldsymbol{\Theta}^t) &= \text{diag}\begin{bmatrix} e^{j\mu_1^t} & \cdots & e^{j\mu_{\hat{K}}^t} \end{bmatrix} \\ \text{eig}(\boldsymbol{\Theta}^d) &= \text{diag}\begin{bmatrix} e^{j\nu_1} & \cdots & e^{j\nu_{\hat{K}}} \end{bmatrix} \end{aligned} \tag{21}$$

where $\text{eig}(\mathbf{A})$ denotes the eigenvalues of $\mathbf{A}$, $\mu_k^r = 2\pi\delta r \sin\theta_k^r$, and $\mu_k^t = 2\pi\delta t \sin\theta_k^t$. The solutions to the equations in (20) are

then obtained using the LS approach, i.e.,

$$\begin{aligned}\boldsymbol{\Theta}^r &= \left((J_{r2}\mathbf{U}_s)^H (J_{r2}\mathbf{U}_s)\right)^{-1} (J_{r2}\mathbf{U}_s)^H (J_{r1}\mathbf{U}_s)\\ \boldsymbol{\Theta}^t &= \left((J_{t2}\mathbf{U}_s)^H (J_{t2}\mathbf{U}_s)\right)^{-1} (J_{t2}\mathbf{U}_s)^H (J_{t1}\mathbf{U}_s)\\ \boldsymbol{\Theta}^d &= \left((J_{d2}\mathbf{U}_s)^H (J_{d2}\mathbf{U}_s)\right)^{-1} (J_{d2}\mathbf{U}_s)^H (J_{d1}\mathbf{U}_s). \end{aligned} \quad (22)$$

It should be noted that, although estimates of the AOAs, AODs, and normalized Doppler shifts can be obtained directly from solutions of (22), an additional algorithm to pair the estimates is required. Typically, pairing of multiple parameter estimates is achieved by using joint Schur decomposition [39], [40] or simultaneous diagonalization [41], [42]. These schemes, however, significantly increase the complexity of the algorithm. Instead, automatic pairing of the estimates is achieved in this paper using a scheme similar to the mean eigenvalue decomposition (MEVD) [43]. Denoting

$$\boldsymbol{\Theta} = \boldsymbol{\Theta}^r + \boldsymbol{\Theta}^t + \boldsymbol{\Theta}^d \quad (23)$$

we eigendecompose $\boldsymbol{\Theta}$ to obtain the common eigenvectors of the three matrices in the sum as

$$\boldsymbol{\Theta} = \mathbf{T}\boldsymbol{\Lambda}\mathbf{T}^{-1}. \quad (24)$$

The diagonal eigenvalue matrices are then computed using

$$\begin{aligned}\mathbf{Z}_r &= \mathbf{T}^{-1}\boldsymbol{\Theta}^r\mathbf{T}\\ \mathbf{Z}_t &= \mathbf{T}^{-1}\boldsymbol{\Theta}^t\mathbf{T}\\ \mathbf{Z}_d &= \mathbf{T}^{-1}\boldsymbol{\Theta}^d\mathbf{T}\end{aligned} \quad (25)$$

where $\mathbf{Z}_r = \mathrm{eig}(\boldsymbol{\Theta}^r)$, $\mathbf{Z}_t = \mathrm{eig}(\boldsymbol{\Theta}^t)$, and $\mathbf{Z}_d = \mathrm{eig}(\boldsymbol{\Theta}^d)$. Estimates of the parameters are obtained from (21) as

$$\begin{aligned}\boldsymbol{\theta}^r &= \mathrm{asin}\left(\frac{-\arg\left(\mathrm{diag}(\mathbf{Z}_r)\right)}{2\pi\delta r}\right)\\ \boldsymbol{\theta}^t &= \mathrm{asin}\left(\frac{-\arg\left(\mathrm{diag}(\mathbf{Z}_t)\right)}{2\pi\delta t}\right)\\ \boldsymbol{\omega} &= \arg\left(\frac{\mathrm{diag}(\mathbf{Z}_d)}{\Delta t}\right)\end{aligned} \quad (26)$$

where $\arg(\cdot)$ denotes the phase of the associated complex number in the range $[0, 2\pi[$.

D. Amplitude Estimation

We assume that, after factoring out the steering vectors $\mathbf{a}_r$ and $\mathbf{a}_t$ in (4), the complex amplitudes β_k of each multipath component are equal for all antenna pairs. We can thus utilize the first entry of the MIMO channel matrix for amplitude estimation. Owing to the Vandermode structure of the array steering matrix, the first entry of $\mathbf{H}(\ell)$ can be modeled as

$$\hat{h}_{11}(\ell) = \sum_{k=1}^{\hat{K}} \beta_k \exp\left(j(\ell-1)\omega_k\Delta t\right) \quad \forall\, \ell \in [1, L]. \quad (27)$$

The following sets of linear equations can therefore be formed using the K available samples

$$\begin{bmatrix}\hat{h}_{11}(1)\\ \vdots\\ \hat{h}_{11}(L)\end{bmatrix} = \begin{bmatrix}1 & \cdots & 1\\ \vdots & \vdots & \ddots & \vdots\\ v_1^{(L-1)} & \cdots & v_{\hat{K}}^{(L-1)}\end{bmatrix}\begin{bmatrix}\beta_1\\ \vdots\\ \beta_{\hat{K}}\end{bmatrix} + \mathbf{z} \quad (28)$$

with a matrix representation given by

$$\hat{\mathbf{h}}_{11} = \mathbf{V}\boldsymbol{\beta} + \mathbf{z}. \quad (29)$$

The definitions of $\hat{\mathbf{h}}_{11}$, $\mathbf{V}$, and $\boldsymbol{\beta}$ follow from (28). The complex amplitudes of the $\hat{K}$ paths are then obtained via an LS solution

$$\begin{aligned}\boldsymbol{\beta} &= \left(\mathbf{V}^H\mathbf{V}\right)^{-1}\mathbf{V}^H\hat{\mathbf{h}}_{11}\\ &= \mathbf{V}^{\dagger}\hat{\mathbf{h}}_{11}\end{aligned} \quad (30)$$

where $(\cdot)^{\dagger}$ denotes the Moore–Penrose pseudoinverse. Although the complex amplitude is estimated using only the first entry of the MIMO channel, the prediction performance can be further improved by using all the entries of the channel matrix for the estimation. However, a compromise has to be made between the performance improvement and complexity reduction since the complexity of amplitude estimation using all matrix entries grows with the number of antenna elements.

E. Mobile Velocity Estimation

A simple scheme for the extraction of the mobile velocities from the estimated multipath parameters is presented here. Given the $\hat{K}$ estimates of the channel parameters $\hat{\omega}_k$, $\hat{\theta}_k^t$, and $\hat{\theta}_k^{\mathrm{r}}$, we use (7) to form

$$\begin{bmatrix}\hat{\omega}_1\\ \hat{\omega}_2\\ \vdots\\ \hat{\omega}_{\hat{K}}\end{bmatrix} = \begin{bmatrix}\cos\left(\theta_1^t\right) & \cos\left(\theta_1^r\right)\\ \cos\left(\theta_2^t\right) & \cos\left(\theta_2^r\right)\\ \vdots & \vdots\\ \cos\left(\theta_{\hat{K}}^t\right) & \cos\left(\theta_{\hat{K}}^r\right)\end{bmatrix}\begin{bmatrix}V_{\max}^t\\ V_{\max}^r\end{bmatrix} \quad (31)$$

where $V_{\max}^t$ and $V_{\max}^r$ denote the maximum Doppler frequencies of the transmitter and receiver, respectively. Solving (31) yields estimates of the maximum Doppler frequencies as

$$\hat{\mathbf{V}}_{\max} = \left(\mathbf{E}^H\mathbf{E}\right)^{-1}\mathbf{E}^H\hat{\boldsymbol{\omega}} \quad (32)$$

where $\hat{\boldsymbol{\omega}} = [\hat{\omega}_1, \ldots, \hat{\omega}_{\hat{K}}]^T$, $\hat{\mathbf{V}}_{\max} = [\hat{V}_{\max}^t\ \hat{V}_{\max}^r]^T$ is a vector containing the Doppler frequencies, and $\mathbf{E}$ is the $\hat{K} \times 2$ matrix

in (31). The mobile velocities can then be calculated from the Doppler estimates using

$$\hat{v}_t = \frac{c\hat{V}^t_{\max}}{2\pi f_{\rm c}}$$
$$\hat{v}_r = \frac{c\hat{V}^r_{\max}}{2\pi f_{\rm c}} \tag{33}$$

where c is the speed of light, and $f_{\rm c}$ is the carrier frequency.

F. Channel Prediction

Following the estimation of all parameters in (8), extrapolation of the CSI is achieved by substitution into the model for the desired prediction horizon. The predicted impulse response is thus

$$\tilde{\mathbf{H}}(\tau) = \sum_{k=1}^{\hat{K}} \hat{\beta}_k \mathbf{a}_r\left(\hat{\theta}^r_k\right) \mathbf{a}^T_t\left(\hat{\theta}^t_k\right) e^{j\tau\hat{\omega}_k} \tag{34}$$

where τ is the desired time instant.

V. Performance Bounds

We now derive the lower bound on the prediction error for MIMO M-to-M wireless channels. Although a derivation of the error bound on narrow-band MIMO F-to-M channel prediction has been presented in [22], the mobility of the transmitter in M-to-M scenarios necessitates the need for an additional parameter in the characterization of the channel and the derivation of the error bound. Moreover, our formulations are simpler than those in [22]. We thus introduce the transmit Doppler frequency and derive prediction error bounds for M-to-M channels here. To emphasize the dependence on transmit Doppler frequency, we express the model in (12) as

$$\mathbf{h}(\ell) = \sum_{k=1}^{K} \beta_k \mathbf{a}_r\left(\mu^r_k\right) \otimes \mathbf{a}_t\left(\mu^t_k\right) e^{j(\ell-1)\left(\nu^r_k+\nu^t_k\right)} \tag{35}$$

and arrange the L observations into an $NML \times 1$ vector $\mathbf{h} = [\mathbf{h}(1) \quad \mathbf{h}(2) \ \cdots \ \mathbf{h}(L)]$. Using (35), $\mathbf{h}$ can be expressed as

$$\mathbf{h} = \sum_{k=1}^{K} \beta_k \mathbf{a}_r\left(\mu^r_k\right) \otimes \mathbf{a}_t\left(\mu^t_k\right) \otimes \mathbf{a}_d\left(\nu^r_k, \nu^t_k\right) \tag{36}$$

where

$$\mathbf{a}_d\left(\nu^r_k, \nu^t_k\right) = \left[1 \quad e^{j(\nu^r_k+\nu^t_k)} \ \cdots \ e^{j(L-1)(\nu^r_k+\nu^t_k)}\right]^T. \tag{37}$$

A more useful representation of (36) is

$$\mathbf{h} = (\mathbf{A}_r \diamond \mathbf{A}_t \diamond \mathbf{A}_d)\boldsymbol{\beta} = \mathbf{A}(\boldsymbol{\Phi})\boldsymbol{\beta} \tag{38}$$

where $\diamond$ denotes the Khatri–Rao product, and $\mathbf{A}_r = [\mathbf{a}_r(\mu^r_1) \quad \mathbf{a}_r(\mu^r_2) \quad \cdots \quad \mathbf{a}_r(\mu^r_K)]$ with $\mathbf{A}_t$ and $\mathbf{A}_d$ defined analogously. We assume that the $6K$ parameter set $\boldsymbol{\Phi} = [\Re(\boldsymbol{\beta}) \quad \Im(\boldsymbol{\beta}) \quad \boldsymbol{\mu}^r \quad \boldsymbol{\mu}^t \quad \boldsymbol{\nu}^r \quad \boldsymbol{\nu}^t]$ is estimated using the L samples available from channel estimation or measurement and subsequently used to extrapolate the channel, as discussed in Section IV. The prediction error at the lth time instant is thus

$$\begin{aligned}\boldsymbol{\epsilon}(\ell) &= \tilde{\mathbf{h}}(\ell, \hat{\boldsymbol{\Phi}}) - \mathbf{h}(\ell, \boldsymbol{\Phi}) \\ &= \sum_{k=1}^{K} \hat{\beta}_k \mathbf{a}_r\left(\hat{\mu}^r_k\right) \otimes \mathbf{a}_t\left(\hat{\mu}^t_k\right) e^{j\ell\left(\hat{\nu}^r_k+\hat{\nu}^t_k\right)} \\ &\quad - \sum_{k=1}^{K} \beta_k \mathbf{a}_r\left(\mu^r_k\right) \otimes \mathbf{a}_t\left(\mu^t_k\right) e^{j\ell\left(\nu^r_k+\nu^t_k\right)}\end{aligned} \tag{39}$$

where $\tilde{\mathbf{h}}$ denotes the predicted channel. Clearly, the prediction error represents a nonlinear continuous function of the channel parameters. The bound on the error covariance $\mathbf{C}_{\epsilon\epsilon}(\ell)$ may therefore be found using the vector form of the CRLB for functions of parameters [44] as

$$\mathbf{C}_{\epsilon\epsilon}(\ell) \geq \frac{\partial \mathbf{h}(\ell, \boldsymbol{\Phi})}{\partial \boldsymbol{\Phi}} \mathbf{Q}^{-1}(\boldsymbol{\Phi}) \frac{\partial \mathbf{h}(\ell, \boldsymbol{\Phi})}{\partial \boldsymbol{\Phi}}^H \tag{40}$$

where

$$\frac{\partial \mathbf{h}(\ell, \boldsymbol{\Phi})}{\partial \boldsymbol{\Phi}} = \left[\frac{\partial \mathbf{h}(\ell, \boldsymbol{\Phi})}{\partial \Phi_1} \quad \cdots \quad \frac{\partial \mathbf{h}(\ell, \boldsymbol{\Phi})}{\partial \Phi_{6K}}\right]^T \tag{41}$$

and $\mathbf{Q}(\boldsymbol{\Phi})^{-1}$ gives the Cramer–Rao bound on the estimation of the channel parameters. Entries of the Fisher information matrix (FIM) may be found using Bang's formula [44] as

$$[\mathbf{Q}(\boldsymbol{\Phi})]_{ij} = \mathrm{Tr}\left[\mathbf{C}^{-1}\frac{\partial \mathbf{C}}{\partial \boldsymbol{\Phi}_i}\mathbf{C}^{-1}\frac{\partial \mathbf{C}}{\partial \boldsymbol{\Phi}_j}\right] + 2\,\mathrm{Re}\left[\frac{\partial \mathbf{h}^H}{\partial \boldsymbol{\Phi}_i}\mathbf{C}^{-1}\frac{\partial \mathbf{h}}{\partial \boldsymbol{\Phi}_j}\right] \tag{42}$$

where $\mathbf{C} = \sigma^2\mathbf{I}$ is the error covariance matrix. Following simplifications, the FIM is found to be[2]

$$[\mathbf{Q}(\Phi)] = \frac{2}{\sigma^2}\Re\left[\mathbf{J}\right] \tag{43}$$

where $\Re[\cdot]$ denotes the real part of the associated complex number, and $\mathbf{J}$ is given by

$$\mathbf{J} = \left(\mathbf{P}^H_5\mathbf{P}_5\right) \odot \left(\mathbf{P}^H_4\mathbf{P}_4\right) \odot \left(\mathbf{P}^H_3\mathbf{P}_3\right) \odot \left(\mathbf{P}^H_2\mathbf{P}_2\right) \odot \left(\mathbf{P}^H_1\mathbf{P}_1\right) \tag{44}$$

where $\odot$ denotes the Hadamard product. The matrices $\mathbf{P}_1$–$\mathbf{P}_5$ are defined as

$$\mathbf{P}_1 = \left[\boldsymbol{\beta}^T \quad \boldsymbol{\beta}^T \quad \boldsymbol{\beta}^T \quad \boldsymbol{\beta}^T \quad \mathbf{1}^1 \quad j\mathbf{1}^T\right] \tag{45}$$

$$\mathbf{P}_2 = [\mathbf{D}_r \quad \mathbf{A}_r \quad \mathbf{A}_r \quad \mathbf{A}_r \quad \mathbf{A}_r \quad \mathbf{A}_r] \tag{46}$$

$$\mathbf{P}_3 = [\mathbf{A}_t \quad \mathbf{D}_t \quad \mathbf{A}_t \quad \mathbf{A}_t \quad \mathbf{A}_t \quad \mathbf{A}_t] \tag{47}$$

$$\mathbf{P}_4 = [\mathbf{A}_d \quad \mathbf{A}_d \quad \mathbf{D}^r_d \quad \mathbf{A}_d \quad \mathbf{A}_d \quad \mathbf{A}_d] \tag{48}$$

$$\mathbf{P}_5 = \left[\mathbf{A}_d \quad \mathbf{A}_d \quad \mathbf{A}_d \quad \mathbf{D}^t_d \quad \mathbf{A}_d \quad \mathbf{A}_d\right] \tag{49}$$

[2]Details of the mathematical derivations are presented in Appendix A.

where $\mathbf{D}_r$, $\mathbf{D}_t$, $\mathbf{D}_d^r$, and $\mathbf{D}_d^t$ are given by

$$\begin{aligned}\mathbf{D}_r &= -j\mathbf{\Gamma}_N\mathbf{A}_r\\ \mathbf{D}_t &= -j\mathbf{\Gamma}_M\mathbf{A}_t\\ \mathbf{D}_d^r &= j\mathbf{\Gamma}_L\mathbf{A}_d\\ \mathbf{D}_d^t &= j\mathbf{\Gamma}_L\mathbf{A}_d\end{aligned} \tag{50}$$

with $\mathbf{\Gamma}_z$ being the diagonal matrix

$$\mathbf{\Gamma}_z = \text{diag}[0 \quad 1 \quad \cdots \quad z-1]. \tag{51}$$

Using (40) and (43), the bound on the prediction MSE can be obtained.

VI. Numerical Simulations

Here, we evaluate the performance of the channel prediction algorithm described in Section IV for different propagation scenarios. The performance metric used in our simulations is the normalized MSE (NMSE) criterion defined as [45, eq. (14)]

$$\text{NMSE}(\tau) = \frac{\mathbb{E}\left[\left\|\tilde{\mathbf{H}}(\tau) - \mathbf{H}(\tau)\right\|_F^2\right]}{\mathbb{E}\left[\|\mathbf{H}(\tau)\|_F^2\right]} \tag{52}$$

where $\mathbf{H}$ is the synthesized or measured channel, and $\|\cdot\|_F$ is the Frobenius norm. The expectations in (52) are computed by averaging over 1000 independent realizations of the channel and/or noise.

A. Simulation Parameters

We consider a ULA at both the transmitter and the receiver. The carrier frequency for the transmission is $f_c = 2.0$ GHz, and the velocities of the transmitter and receiver are, respectively, $v_t = 25$ km/h and $v_r = 50$ km/h. The fading amplitudes β_k are generated as complex Gaussian distributed random variables $\beta_k \sim \mathcal{CN}(0,1)$. The AoA and AoD are assumed uniformly distributed, i.e., θ_k^r and $\theta_k^t \sim \mathcal{U}[-\pi, \pi[$. Similarly, the AoA and AoD relative to the directions of motion are ϑ_k^r, $\vartheta_k^t \sim \mathcal{U}[-\pi, \pi[$. Based on the parameter distributions, it can be shown that the average power of a K path channel is $\mathbb{E}[\|\mathbf{H}(\tau)\|_F^2] = NMK$. To allow a comparison of the NMSE in (52) with the derived bound, we define the NMSE bound (NMSEB) as

$$\text{NMSEB}(\tau) = \frac{\text{Tr}\left[\mathbf{C}_{\epsilon\epsilon}(\tau)\right]}{NMK} \tag{53}$$

where $\text{Tr}[\cdot]$ denotes the sum of the diagonal elements of the associated matrix. Except where otherwise stated, the prediction is based on $L = 100$ samples with a sampling interval of $\Delta t = 2$ ms.

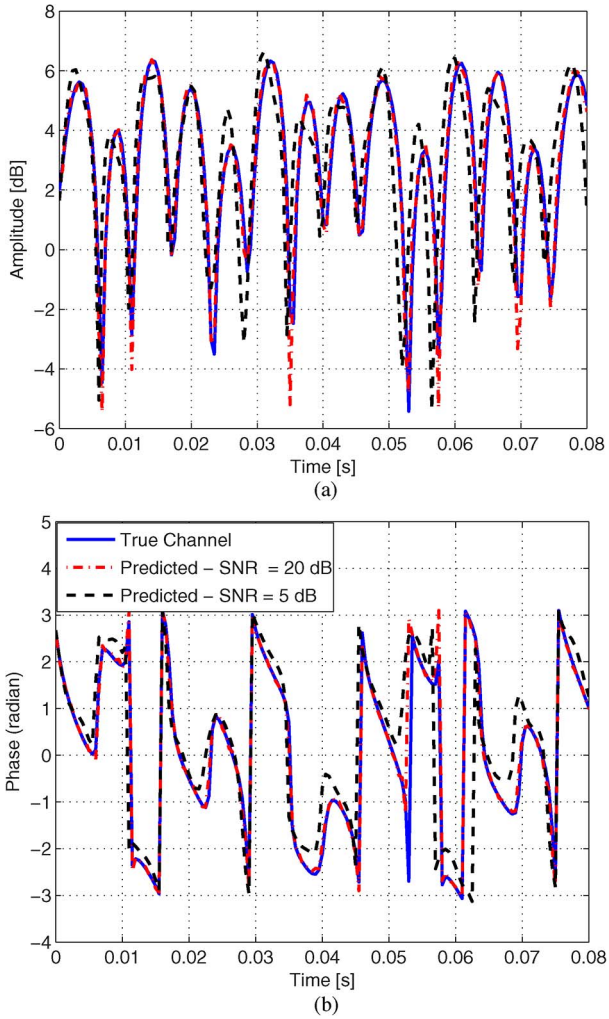

Fig. 2. Plot of the actual and predicted channels of a 2×2 MIMO M-to-M system at SNR $= [5, 20]$ dB. (a) Amplitude. (b) Phase.

B. Prediction Performance Evaluation

We consider a scenario with $K = 8$ paths.[3] In Fig. 2, we plot the time-varying amplitude and phase of the actual and predicted channel for the first entry of a 2×2 MIMO M-to-M system at SNR $= [5, 20]$ dB. We observe that the proposed algorithm yields very good prediction of both the amplitude and phase of the channel at both SNR values except for instances of deep fades. We also observe that while the instant of deep fades and peaks are accurately predicted at SNR $= 20$ dB, the predicted deep fades at 5 dB has a small time lag (< 1 ms) when compared with the actual channel amplitude. As expected, the predicted phase of the channel is also more accurate at 20 dB. The prediction performance is quantified in Fig. 3, where we present the normalized mean square prediction error and error bound versus prediction horizon for a 2×2 MIMO channel at SNR $= [5, 20]$ dB. As expected, the prediction error increases with the prediction interval and decreases with SNR. We observe that the performance of the proposed method is closer to

[3]It has been shown in [46] that outdoor environments are characterized by few dominant scatterers and that the channel can be described by three to eight distinct paths.

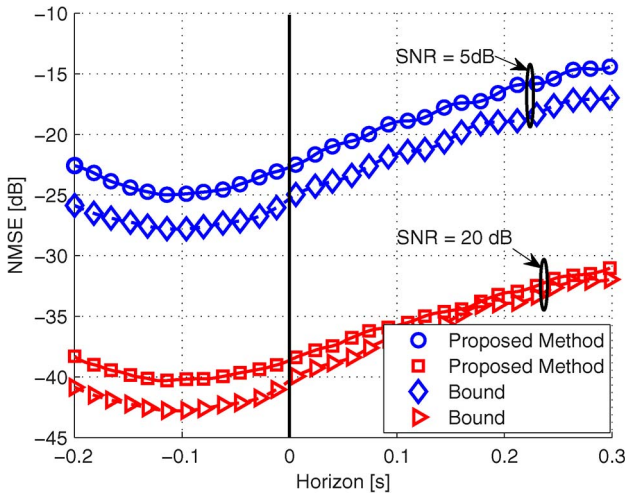

Fig. 3. NMSE and NMSEB versus prediction horizon for the prediction of a 2×2 MIMO M-to-M channel at different SNR levels. Prediction starts after the vertical line.

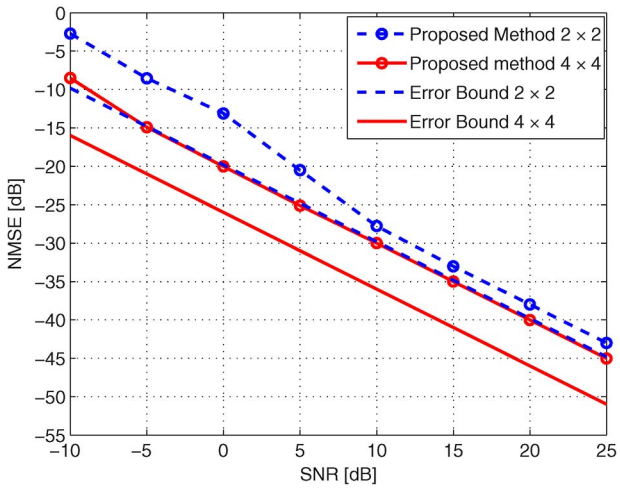

Fig. 5. NMSE and NMSEB versus SNR for a prediction horizon of $\tau = 10$ ms with different numbers of antennas.

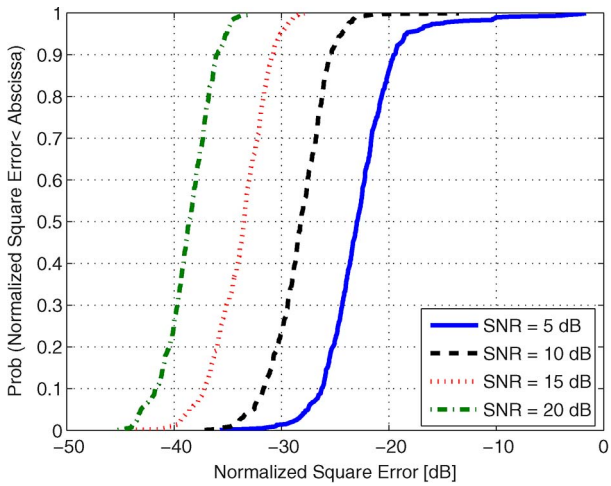

Fig. 4. CDF of prediction NSE for a prediction horizon of 10 ms at SNR $= [5, 10, 15, 20]$ dB.

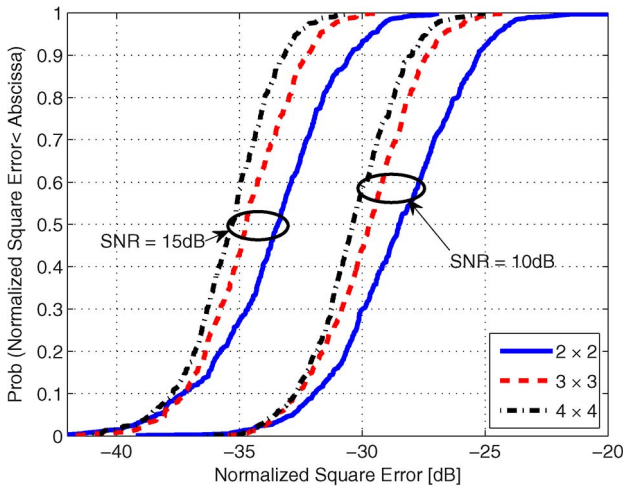

Fig. 6. CDF of NSE for a prediction horizon of 10 ms at SNR $= [10, 15]$ dB for 2×2, 3×3, and 4×4 MIMO M-to-M channels.

the bound at SNR $= 20$ dB. In Fig. 4, we show the cumulative distribution function (cdf) of the normalized squared prediction error at $\tau = 10$ ms. The cdf curves clearly show that, as SNR increases, the NMSE of the proposed algorithm decreases.

In Fig. 5, we plot the NMSE and NMSEB versus SNR for different numbers of antenna elements and prediction horizon of $\tau = 10$ ms. We observe that increasing the number of transmit and receive antenna elements offers more information about the propagation channel and thus decreases the NMSE at all SNR values for the prediction horizon considered, with a greater impact at low SNR. We also observe that, for a 2×2 M-to-M channel, the performance of the proposed method approaches the lower bound as the SNR increases. The corresponding cdfs of normalized square error (NSE) are shown in Fig. 6, which confirms the results for mean error values in Fig. 5.

The effects of the estimation length L on the prediction performance is shown in Fig. 7. We observe that, at SNR $=$ 10 dB, $L = 100$ is required to approach the NMSEB, with a much greater number needed at a lower SNR. Approaching the

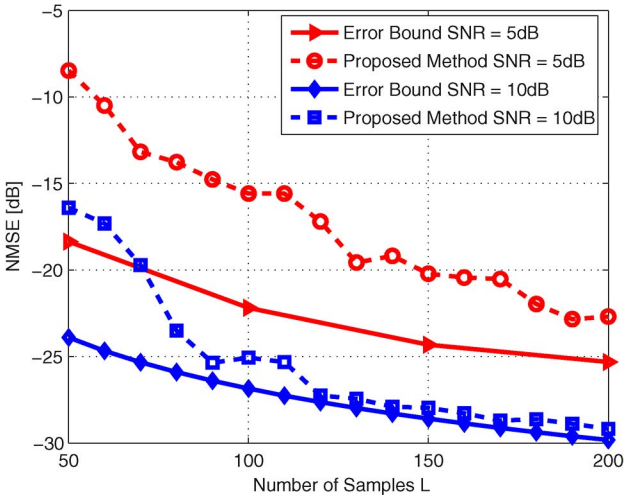

Fig. 7. NMSE and NMSEB versus training length (number of known samples) for a 2×2 MIMO M-to-M channel prediction over the horizon of $\tau = 20$ ms at SNR $= [5, 10]$ dB.

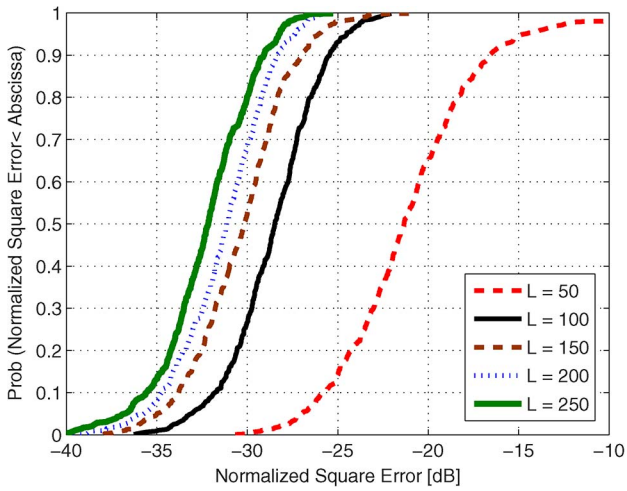

Fig. 8. CDF of NSE for a prediction horizon of $\tau = 10$ ms at SNR $= 10$ dB.

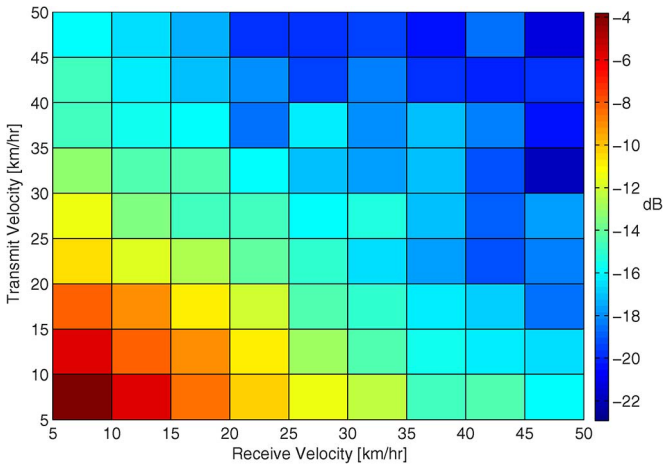

Fig. 9. Effects of transmitter and receiver velocity on prediction NMSE at SNR $= 5$ dB.

NMSEB as the number of samples increases is expected since subspace-based schemes are asymptotic maximum likelihood estimators. A similar observation is made in Fig. 8, where we present the cdf of NSE at $\tau = 10$ ms. Finally, we illustrate the effect of transmitter and receiver velocity on the prediction NMSE at an interval of $\tau = 10$ ms in Fig. 9. It shows that, as the transmitter and/or receiver velocity increases, the prediction NMSE decreases. This is intuitively satisfying since increased velocity results in longer spatial distance over the same training interval, thereby revealing more structure of the channel.

C. Mobile Velocity Estimation Error

The performance of the proposed mobile velocity estimation algorithm described in Section IV-E is evaluated in terms of the root mean square error (RMSE) defined as

$$\mathrm{RMSE}(v_{\mathrm{t/r}}) = \sqrt{\frac{1}{C}\sum_{c=1}^{C}\left(v_{\mathrm{t/r}} - \hat{v}_{\mathrm{t/r}}(c)\right)^2} \qquad (54)$$

where C is the number of Monte Carlo simulations. In Fig. 10, we plot the RMSE versus SNR for both the transmit and

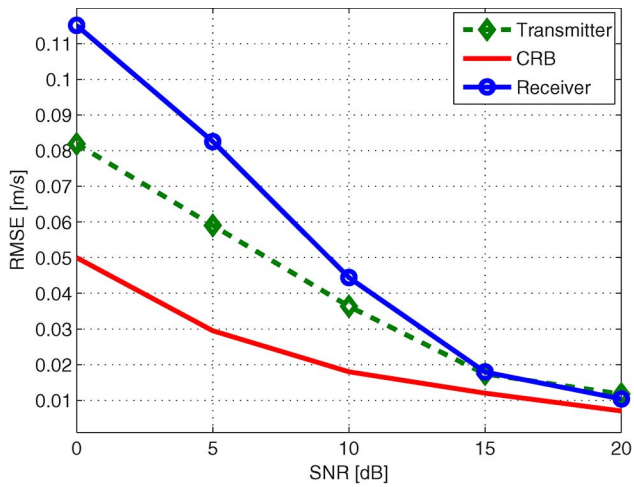

Fig. 10. Mobile velocity estimation RMSE versus SNR for 2×2 MIMO M-to-M channel with $K = 2$ propagation paths.

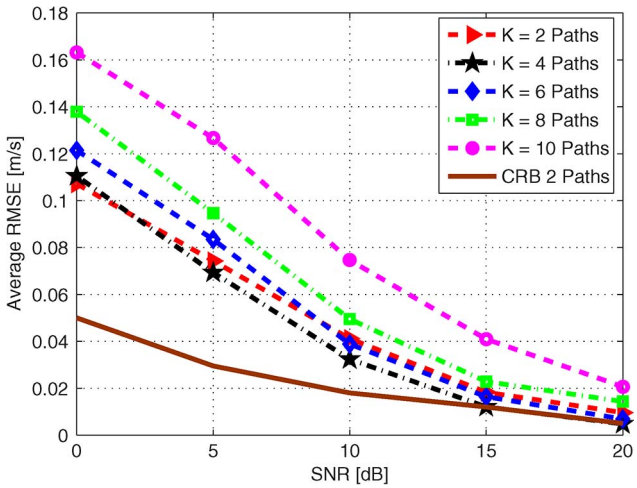

Fig. 11. Mobile velocity estimation RMSE versus SNR for 2×2 MIMO M-to-M channel with different numbers of propagation paths.

receive mobile velocity estimation and compare with the square root of the Cramer–Rao bound on velocity estimates (obtained from the diagonal entries of the inverse of (43) corresponding to Doppler frequency estimates). As expected, the RMSE decreases and approaches the bound with increasing SNR. Fig. 11 shows the effect of the number of propagation paths on the averaged velocity estimation accuracy. The RMSE values presented are the average of those for v_r and v_t. As shown in the figure, increasing the number of paths K from two to four decreases the RMSE. However, the RMSE increases for $K > 4$. A plausible explanation for this is that, although an increase in the number of paths is expected to improve the accuracy of the LS velocity estimation, the channel parameter estimates become less accurate as the number of paths increases. This shows that the performance of the velocity estimation stage is dependent on the accuracy of the channel parameter estimates with more accurate parameter estimates, leading to improved velocity estimation.

Finally, we illustrate the effect of the transmitter and receiver velocity on the averaged RMSE performance in Fig. 12, where

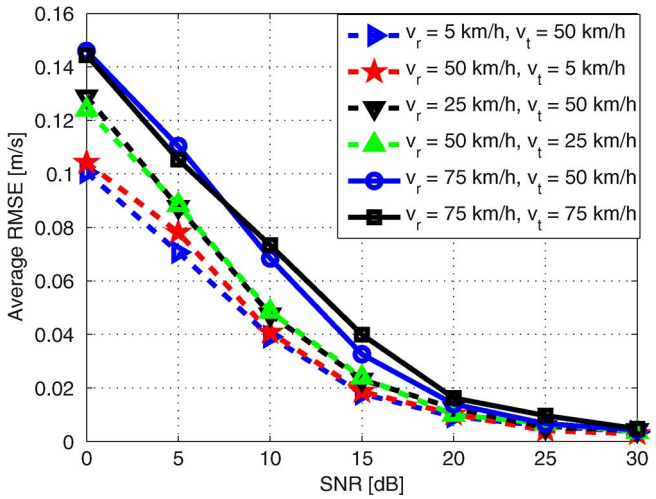

Fig. 12. Averaged RMSE versus SNR for different values of v_r and v_r for a 2×2 M-to-M channel with $K = 6$ paths.

we plot the averaged velocity estimation RMSE versus SNR for different values of v_t and v_r. We observe that an increase in velocity increases the RMSE at low SNR values. However, the RMSE values when normalized by the total velocity are of the same order of magnitude for all velocity values plotted.

VII. Conclusion

In this paper, we performed a detailed investigation of the prediction of MIMO M-to-M wireless communication channels. Starting with a statistical model for M-to-M channels, we derived a parametrized model for jointly estimating the AOA, AOD, and effective Doppler frequency shifts via a 3-D extension of the ESPRIT algorithm. We proposed a simple and efficient scheme for the estimation of mobile velocities and derived the bound on the prediction of narrow-band M-to-M channel. Simulation results show that the proposed algorithm offers accurate and long-range prediction and approaches the prediction error bound with increasing SNR and/or number of samples in the measured segment. Future work will analyze the performance of the algorithm on measured data and extend the proposed method to wideband M-to-M MIMO channels.

Appendix A
Derivatives for the Fisher Information Matrix

Here, we present the derivatives of the observation vector $\mathbf{h}$ required for evaluating the FIM expression as given in (44). The derivatives are obtained from (38).

1) Derivative With Respect to $\Re(\boldsymbol{\beta})$:

$$\begin{aligned}\frac{\partial \mathbf{h}}{\partial \Re(\beta_k)} &= \frac{\partial (\mathbf{A}_r \diamond \mathbf{A}_t \diamond \mathbf{A}_d)\boldsymbol{\beta}}{\partial \Re(\beta_k)} \\ &= (\mathbf{A}_r \diamond \mathbf{A}_t \diamond \mathbf{A}_d)\frac{\partial \boldsymbol{\beta}}{\partial \beta_k} \\ &= (\mathbf{A}_r \diamond \mathbf{A}_t \diamond \mathbf{A}_d)\boldsymbol{\Pi}_K \end{aligned} \tag{55}$$

where $\boldsymbol{\Pi}_k$ is a $K \times 1$ vector having a 1 as the kth element and all other elements as zero. Equation (55) can further be simplified to

$$\begin{aligned}\frac{\partial \mathbf{h}}{\partial \Re(\beta_k)} &= [\mathbf{A}_r]_{:,k} \otimes [\mathbf{A}_t]_{:,k} \otimes [\mathbf{A}_d]_{:,k} \\ &= [\mathbf{A}_r \diamond \mathbf{A}_t \diamond \mathbf{A}_d]_{:,k} \\ &= [\mathbf{A}]_{:,k} \end{aligned} \tag{56}$$

where $[\mathbf{B}]_{:,k}$ denotes the kth column of $\mathbf{B}$. Using (56), the derivative with respect to $\Re(\boldsymbol{\beta})$ is

$$\begin{aligned}\frac{\partial \mathbf{h}}{\partial \Re(\boldsymbol{\beta})} &= \left[\frac{\partial \mathbf{h}}{\partial \Re(\beta_1)} \quad \frac{\partial \mathbf{h}}{\partial \Re(\beta_2)} \quad \cdots \quad \frac{\partial \mathbf{h}}{\partial \Re(\beta_K)}\right] \\ &= [[\mathbf{A}]_{:,1} \quad \cdots \quad [\mathbf{A}]_{:,K}] \\ &= \mathbf{A}. \end{aligned} \tag{57}$$

2) Derivative With Respect to $\Im(\boldsymbol{\beta})$:

$$\begin{aligned}\frac{\partial \mathbf{h}}{\partial \Im(\beta_k)} &= (\mathbf{A}_r \diamond \mathbf{A}_t \diamond \mathbf{A}_d)\frac{\partial \boldsymbol{\beta}}{\partial \Im(\beta_k)} \\ &= j(\mathbf{A}_r \diamond \mathbf{A}_t \diamond \mathbf{A}_d)\boldsymbol{\Pi}_K \\ &= j\mathbf{A}. \end{aligned} \tag{58}$$

3) Derivative With Respect to $\boldsymbol{\mu}^r$:

$$\begin{aligned}\frac{\partial \mathbf{h}}{\partial \mu_k^r} &= \left(\frac{\partial \mathbf{A}_r}{\partial \mu_k^r} \diamond \mathbf{A}_t \diamond \mathbf{A}_d\right)\boldsymbol{\beta} \\ &= \left(\frac{\partial [\mathbf{A}_r]_{:,k}}{\partial \mu_k^r} \otimes [\mathbf{A}_t]_{:,k} \otimes [\mathbf{A}_d]_{:,k}\right)\beta_k. \end{aligned} \tag{59}$$

Using (60), we obtain

$$\begin{aligned}\frac{\partial \mathbf{h}}{\partial \boldsymbol{\mu}^r} &= \left[\frac{\partial \mathbf{h}}{\partial \mu_1^r} \quad \frac{\partial \mathbf{h}}{\partial \mu_2^r} \quad \cdots \quad \frac{\partial \mathbf{h}}{\partial \mu_K^r}\right] \\ &= \left[\left(\frac{\partial [\mathbf{A}_r]_{:,1}}{\partial \mu_1^r} \otimes [\mathbf{A}_t]_{:,1} \otimes [\mathbf{A}_d]_{:,1}\right)\beta_1 \quad \cdots \right. \\ &\qquad \left. \left(\frac{\partial [\mathbf{A}_r]_{:,K}}{\partial \mu_K^r} \otimes [\mathbf{A}_t]_{:,K} \otimes [\mathbf{A}_d]_{:,K}\right)\beta_K\right] \\ &= (\mathbf{D}_r \diamond \mathbf{A}_t \diamond \mathbf{A}_d)\mathbf{X} \end{aligned} \tag{60}$$

where

$$\mathbf{D}_r = \left[\frac{\partial [\mathbf{A}_r]_{:,1}}{\partial \mu_1^r} \quad \frac{\partial [\mathbf{A}_r]_{:,2}}{\partial \mu_2^r} \quad \cdots \quad \frac{\partial [\mathbf{A}_r]_{:,K}}{\partial \mu_K^r}\right]. \tag{61}$$

For the ULA, $\mathbf{D}_r$ can be found using (5) to be

$$\mathbf{D}_r = \begin{bmatrix} 0 & \cdots & 0 \\ je^{j\nu_1^r} & \cdots & je^{j\nu_K^r} \\ 2je^{j2\nu_1^r} & \cdots & 2je^{j2\nu_K^r} \\ \vdots & \ddots & \vdots \\ j(N-1)e^{j(N-1)\nu_1^r} & \cdots & j(N-1)e^{j(N-1)\nu_K^r} \end{bmatrix}. \tag{62}$$

Equation (62) can be expressed in terms of $\mathbf{A}_r$ as

$$\mathbf{D}_r = j\begin{bmatrix} 0 & 0 & \cdots & 0 \\ 0 & 1 & \cdots & 0 \\ \vdots & \vdots & \ddots & \vdots \\ 0 & 0 & \cdots & (N-1) \end{bmatrix}\mathbf{A}_r. \tag{63}$$

$\mathbf{X}$ is a diagonal matrix with the complex amplitudes $\boldsymbol{\beta}$ on its diagonal.

4) Derivative With Respect to $\boldsymbol{\mu}^t$:

$$\begin{aligned}\frac{\partial \mathbf{h}}{\partial \boldsymbol{\mu}^t} &= \left[\frac{\partial \mathbf{h}}{\partial \mu_1^t} \quad \frac{\partial \mathbf{h}}{\partial \mu_2^t} \quad \cdots \quad \frac{\partial \mathbf{h}}{\partial \mu_K^t}\right] \\ &= \left[\left([\mathbf{A}_r]_{:,1} \otimes \frac{\partial [\mathbf{A}_t]_{:,1}}{\partial \mu_1^t} \otimes [\mathbf{A}_d]_{:,1}\right)\beta_1 \ \cdots \right. \\ &\qquad \left. \left([\mathbf{A}_r]_{:,K} \otimes \frac{\partial [\mathbf{A}_t]_{:,K}}{\partial \mu_K^t} \otimes [\mathbf{A}_d]_{:,K}\right)\beta_K\right] \\ &= (\mathbf{A}_r \diamond \mathbf{D}_t \diamond \mathbf{A}_d)\mathbf{X} \end{aligned} \tag{64}$$

where $\mathbf{D}_t$ is defined similar to $\mathbf{D}_r$.

5) Derivative With Respect to $\boldsymbol{\nu}^t$ and $\boldsymbol{\nu}^r$:

$$\begin{aligned}\frac{\partial \mathbf{h}}{\partial \boldsymbol{\nu}^t} &= \left[\frac{\partial \mathbf{h}}{\partial \nu_1^t} \quad \frac{\partial \mathbf{h}}{\partial \nu_2^t} \quad \cdots \quad \frac{\partial \mathbf{h}}{\partial \nu_K^t}\right] \\ &= \left[\left([\mathbf{A}_r]_{:,1} \otimes [\mathbf{A}_t]_{:,1} \otimes \frac{\partial [\mathbf{A}_d]_{:,1}}{\partial \nu_1^t}\right)\beta_1 \ \cdots \right. \\ &\qquad \left. \left([\mathbf{A}_r]_{:,K} \otimes [\mathbf{A}_t]_{:,K}\right)\beta_K \otimes \frac{\partial [\mathbf{A}_d]_{:,K}}{\partial \nu_K^t}\right] \\ &= \left(\mathbf{A}_r \diamond \mathbf{A}_t \diamond \mathbf{D}_d^t\right)\mathbf{X} \end{aligned} \tag{65}$$

where $\mathbf{D}_d^t$ is defined similar to (62).

APPENDIX B
EVALUATION OF FISHER INFORMATION MATRIX AND ERROR BOUND

The simplified expression for the FIM in (44) and the prediction error bound are obtained using the derivatives in Appendix A. Using (42) and (43), the matrix $\mathbf{J}$ in (44) is given by

$$\mathbf{J} = \frac{\partial \mathbf{h}}{\partial \boldsymbol{\Phi}}^H \frac{\partial \mathbf{h}}{\partial \boldsymbol{\Phi}} \tag{66}$$

where

$$\begin{aligned}\frac{\partial \mathbf{h}}{\partial \boldsymbol{\Phi}} &= \left[\frac{\partial \mathbf{h}}{\partial \Re(\boldsymbol{\Phi})} \quad \frac{\partial \mathbf{h}}{\partial \Im(\boldsymbol{\Phi})} \quad \frac{\partial \mathbf{h}}{\partial \boldsymbol{\mu}^r} \quad \frac{\partial \mathbf{h}}{\partial \boldsymbol{\mu}^t} \quad \frac{\partial \mathbf{h}}{\partial \boldsymbol{\nu}^r} \quad \frac{\partial \mathbf{h}}{\partial \boldsymbol{\nu}^t}\right] \\ &= \left[\mathbf{A} \quad j\mathbf{A} \quad (\mathbf{D}_r \diamond \mathbf{A}_t \diamond \mathbf{A}_d)\mathbf{X} \quad (\mathbf{A}_r \diamond \mathbf{D}_t \diamond \mathbf{A}_d)\mathbf{X} \right. \\ &\qquad \left. (\mathbf{A}_r \diamond \mathbf{A}_t \diamond \mathbf{D}_d^r)\,\mathbf{X} \quad \left(\mathbf{A}_r \diamond \mathbf{A}_t \diamond \mathbf{D}_d^t\right)\mathbf{X}\right]. \end{aligned} \tag{67}$$

With $\mathbf{P}_1$–$\mathbf{P}_5$ given in (46)–(50), (67) can be simplified to

$$\frac{\partial \mathbf{h}}{\partial \boldsymbol{\Phi}} = \mathbf{P}_1 \diamond \mathbf{P}_2 \diamond \mathbf{P}_3 \diamond \mathbf{P}_4 \diamond \mathbf{P}_5 \tag{68}$$

and thus, (66) becomes

$$\mathbf{J} = (\mathbf{P}_1 \diamond \mathbf{P}_2 \diamond \mathbf{P}_3 \diamond \mathbf{P}_4 \diamond \mathbf{P}_5)^H (\mathbf{P}_1 \diamond \mathbf{P}_2 \diamond \mathbf{P}_3 \diamond \mathbf{P}_4 \diamond \mathbf{P}_5). \tag{69}$$

Using the properties of the Khatri–Rao and Hardamad products, (69) reduces to the form given in (44).

REFERENCES

[1] "IEEE P802.11p/D9.0: Part 11: Wireless LAN Medium Access Control (MAC) and Physical Layer (PHY) specifications: Amendment: Wireless Access in Vehicular Environments (WAVE)," IEEE, Piscataway, NJ, USA, Tech. Rep., 2009.

[2] A. S. Akki and F. Haber, "A statistical model of mobile-to-mobile land communication channel," *IEEE Trans. Veh. Technol.*, vol. 35, no. 1, pp. 2–7, Feb. 1986.

[3] A. S. Akki, "Statistical properties of mobile-to-mobile land communication channels," *IEEE Trans. Veh. Technol.*, vol. 43, no. 4, pp. 826–831, Nov. 1994.

[4] F. Vatalaro and A. Forcella, "Doppler spectrum in mobile-to-mobile communications in the presence of three-dimensional multipath scattering," *IEEE Trans. Veh. Technol.,* vol. 46, no. 1, pp. 213–219, Feb. 1997.

[5] J. Maurer, T. Schafer, and W. Wiesbeck, "A realistic description of the environment for inter-vehicle wave propagation modelling," in *Proc. IEEE VTC—Fall*, vol. 3, 2001, pp. 1437–1441.

[6] J. Maurer, T. Fugen, T. Schafer, and W. Wiesbeck, "A new inter-vehicle communications (IVC) channel model," in *Proc. IEEE VTC—Fall*, vol. 1, 2004, pp. 9–13.

[7] G. Acosta, K. Tokuda, and M.-A. Ingram, "Measured joint Doppler-delay power profiles for vehicle-to-vehicle communications at 2.4 GHz," in *Proc. IEEE GLOBECOM*, vol. 6, 2004, pp. 3813–3817.

[8] I. Kovacs, P. C. F. Eggers, K. Olesen, and L. Petersen, "Investigations of outdoor-to-indoor mobile-to-mobile radio communication channels," in *Proc. IEEE VTC—Fall*, vol. 1, 2002, pp. 430–434.

[9] J. Maurer, T. Fugen, and W. Wiesbeck, "Narrow-band measurement and analysis of the inter-vehicle transmission channel at 5.2 GHz," in *Proc. IEEE VTC—Spring*, vol. 3, 2002, pp. 1274–1278.

[10] S. Patel L. Stüber, and T. G. Pratt, "Simulation of Rayleigh-faded mobile-to-mobile communication channels," *IEEE Trans. Commun.*, vol. 53, no. 11, pp. 1876–1884, Nov. 2005.

[11] M. Patzold, B. Hogstad, N. Youssef, and D. Kim, "A MIMO mobile-to-mobile channel model: Part I—The reference model," in *Proc. IEEE PIMRC*, vol. 1, 2005, pp. 573–578.

[12] B. Hogstad, M. Patzold, N. Youssef, and D. Kim, "A MIMO mobile-to-mobile channel model: Part II—The simulation model," in *Proc. IEEE PIMRC*, vol. 1, 2005, pp. 562–567.

[13] A. G. Zajic and G. L. Stuber, "Simulation models for MIMO mobile-to-mobile channels," in *Proc. IEEE MILCOM*, 2006, pp. 1905–1911.

[14] A. G. Zajic and G. L. Stüber, "A three-dimensional MIMO mobile-to-mobile channel model," in *Proc. IEEE WCNC*, 2007, pp. 1883–1887.

[15] A. G. Zajic and G. L. Stüber, "A three dimensional parametric model for wideband MIMO mobile-to-mobile channels," in *Proc. IEEE GLOBECOM*, 2007, pp. 3760–3764.

[16] X. Cheng *et al.*, "An improved parameter computation method for a MIMO V2V Rayleigh fading channel simulator under non-isotropic scattering environments," *IEEE Commun. Lett.*, vol. 17, no. 2, pp. 265–268, Feb. 2013.

[17] A. Molisch, F. Tufvesson, J. Karedal, and C. Mecklenbrauker, "Propagation aspects of vehicle-to-vehicle communications—An overview," in *Proc. IEEE RWS*, 2009, pp. 179–182.

[18] J. Vanderpypen and L. Schumacher, "MIMO channel prediction using ESPRIT based techniques," in *Proc. IEEE PIMRC*, 2007, pp. 1–5.

[19] K. Okino, T. Nakayama, S. Joko, Y. Kusano, and S. Kimura, "Direction based beamspace MIMO channel prediction with ray cancelling," in *Proc. IEEE PIMRC*, 2008, pp. 1–5.

[20] R. Adeogun, P. D. Teal, and P. A. Dmochowski, "Parametric channel prediction for narrowband mobile MIMO systems using spatio-temporal correlation analysis," in *Proc. IEEE VTC—Fall*, 2013, pp. 1–5.

[21] R. O. Adeogun, P. D. Teal, and P. A. Dmochowski, "Parametric channel prediction for narrowband mimo systems using polarized antenna arrays," in *Proc. IEEE Veh. Technol. Conf. Spring*, May 2014, pp. 1–5.

[22] T. Svantesson and A. Swindlehurst, "A performance bound for prediction of MIMO channels," *IEEE Trans. Signal Process.*, vol. 54, no. 2, pp. 520–529, Oct. 2006.

[23] R. O. Adeogun, P. D. Teal, and P. A. Dmochowski, "Novel algorithm for prediction of wideband mobile MIMO wireless channels," in *Proc. IEEE Int. Conf. Commun.*, Jun. 2014, pp. 4632–4637.

[24] A. G. Zajic and G. L. Stüber, "Maximum likelihood method for MIMO mobile-to-mobile channel parameter estimation," in *Proc. GLOBECOM*, 2008, pp. 3969–3973.

[25] A. G. Zajic, "Estimation of velocities in mobile-to-mobile wireless fading channels," in *Proc. IEEE VTC—Fall*, 2011, pp. 1–5.

[26] A. G. Zajic, "Estimation of mobile velocities and direction of movement in mobile-to-mobile wireless fading channels," *IEEE Trans. Veh. Technol.*, vol. 61, no. 1, pp. 130–139, Jan. 2012.
[27] A. Duel-Hallen, "Fading channel prediction for mobile radio adaptive transmission systems," *Proc. IEEE*, vol. 95, no. 12, pp. 2299–2313, Dec. 2007.
[28] A. Duel-Hallen, S. Hu, and H. Hallen, "Long range prediction of fading signals: Enabling adaptive transmission for mobile radio channels," *IEEE Signal Process. Mag.*, vol. 17, no. 3, pp. 62–75, May 2000.
[29] M. Chen and M. Viberg, "Long-range channel prediction based on non-stationary parametric modeling," *Trans. Signal Process.*, vol. 57, no. 2, pp. 622–634, Feb. 2009.
[30] T. Ekman, "Prediction of mobile radio channels—Modeling and design," Ph.D. dissertation, Uppsala Univ., Uppsala, Sweden, 2002.
[31] P. Teal and R. Vaughan, "Simulation and performance bounds for real-time prediction of the mobile multipath channel," in *Proc. IEEE Workshop Statist. Signal Process.*, 2001, pp. 548–551.
[32] M. Chen, T. Ekman, and M. Viberg, "New approaches for channel prediction based on sinusoidal modeling," *EURASIP J. Appl. Signal Process.*, vol. 2007, no. 1, p. 197, Jan 2007.
[33] M. Wax and T. Kailath, "Detection of signals by information theoretic criteria," *IEEE Trans. Acoust., Speech Signal Process.*, vol. ASSP-33, no. 2, pp. 387–392, Apr. 1985.
[34] H. Akaike, "A new look at the statistical model identification," *IEEE Trans. Autom. Control*, vol. AC-19, no. 6, pp. 716–723, Dec. 1974.
[35] L. Huang, T. Long, E. Mao, H. C. So, and S. Member, "MMSE-based MDL method for accurate source number estimation," *IEEE Signal Process. Lett.*, vol. 16, no. 9, pp. 798–801, Sep. 2009.
[36] R. Roy and T. Kailath, "Estimation of signal parameters via rotational invariance techniques," *IEEE Trans. Acoust., Speech, Signal Process.*, vol. 37, no. 7, pp. 984–995, Jul. 1989.
[37] A. Swindlehurst, B. Ottersten, R. Roy, and T. Kailath, "Multiple invariance ESPRIT," *IEEE Trans. Signal Process.*, vol. 40, no. 4, pp. 867–881, Apr. 1992.
[38] K. T. Wong and M. Zoltowski, "Closed-form multi-dimensional multi-invariance ESPRIT," in *Proc. IEEE ICASSP*, 1997, pp. 3489–3492.
[39] M. Haardt and J. Nossek, "Simultaneous Schur decomposition of several nonsymmetric matrices to achieve automatic pairing in multidimensional harmonic retrieval problems," *IEEE Trans. Signal Process.*, vol. 46, no. 1, pp. 161–169, Jan. 1998.
[40] K. Abed-Meraim and Y. Hua, "A least-squares approach to joint schur decomposition," in *Proc. IEEE ICASSP*, vol. 4, 1998, pp. 2541–2544.
[41] T. Fu and X. Gao, "Simultaneous diagonalization with similarity transformation for non-defective matrices," in *Proc. IEEE ICASSP*, vol. 4, 2006, p. IV.
[42] A. Bunse-Gerstner, R. Byers, and V. Mehrmann, "Numerical methods for simultaneous diagonalization," *SIAM J. Matrix Anal. Appl.*, vol. 14, no. 4, pp. 927–949, 1993.
[43] N. Kikuma, H. Kikuchi, and N. Inagaki, "Pairing of estimates using mean eigenvalue decomposition in multi-dimensional unitary ESPRIT," *IEICE Trans*, vol. J82-B, no. 11, pp. 2202–2207, Nov 1999.
[44] S. M. Kay, *Fundamentals of Statistical Signal Processing: Estimation Theory*. Upper Saddle River, NJ, USA: Prentice-Hall, 1993.
[45] S. Zhou and G. Giannakis, "How accurate channel prediction needs to be for transmit-beamforming with adaptive modulation over Rayleigh MIMO channels?" *IEEE Trans. Wireless Commun.*, vol. 3, no. 4, pp. 1285–1294, Jul. 2004.
[46] A. Arredondo, K. R. Dandekar, and G. Xu, "Vector channel modeling and prediction for the improvement of downlink received power," *IEEE Trans. Commun.*, vol. 50, no. 7, pp. 1121–1129, Jul. 2002.

Ramoni O. Adeogun (S'12–M'14) received the B.Eng. degree (with first-class honors) in electrical and computer engineering from the Federal University of Technology Minna, Minna, Nigeria, in 2007. He is currently working toward the Ph.D. degree with the School of Engineering and Computer Science, Victoria University of Wellington, Wellington, New Zealand.

Between 2008 and 2009, he was with the Information and Communication Technology Directorate, University of Jos, Jos, Nigeria. In 2009, he worked briefly as a Telecommunications Engineer with Odua Telecoms Ltd., Ibadan, Nigeria. Since 2010, he has been with the National Space Research and Development Agency (NASRDA), Abuja, Nigeria, where he is currently working with the Engineering and Space Systems Division. His research interests include channel characterization and modeling, adaptive communication, and signal processing for communications.

Dr. Adeogun has received several honors and awards, including the Ogun State Tertiary Scholarship (2003–2006), the Best Graduating Student in the University (2007), and the Victoria Doctoral Scholarship.

Paul D. Teal (M'05–SM'06) received the B.E. degree from the University of Sydney, Sydney, Australia, in 1990 and the Ph.D. degree from the Australian National University, Canberra, Australia, in 2002.

He has been employed in Australia by Telstra and in New Zealand by Concord Technologies, Caravel Consultants, and Industrial Research Limited, in a number of technology development, deployment, consultant, and research roles involving telecommunications infrastructure, industrial telemetry and control, voice processing, and call centers. Since 2006 he has been a Senior Lecturer and an Associate Professor with Victoria University of Wellington, Wellington, New Zealand. His research interests include the development of signal processing algorithms and their application in communications, audio, acoustics, and biomedical devices and on the perception of sound, particularly research on Bayesian tracking, blind source separation, modeling, and machine learning.

Dr. Teal received a University Medal from the University of Sydney for his B.E. degree.

Pawel A. Dmochowski (S'02–M'07–SM'11) was born in Gdansk, Poland. He received the B.A.Sc. degree in engineering physics from The University of British Columbia, Vancouver, BC, Canada, in 1998 and the M.Sc. and Ph.D. degrees from Queen's University, Kingston, ON, Canada, in 2001 and 2006, respectively.

He was a Natural Sciences and Engineering Research Council Visiting Fellow with the Communications Research Centre Canada and a Sessional Instructor with Carleton University, Ottawa, ON, Canada. He is currently a Senior Lecturer with the School of Engineering and Computer Science, Victoria University of Wellington, Wellington, New Zealand. His research interests include cognitive radio, limited feedback, and massive multiple-input–multiple-output systems.

Dr. Dmochowski is actively involved in the IEEE New Zealand Central Section Committee.